

# Multi-object spectroscopy of CL1821+643: a dynamically relaxed cluster with a giant radio halo?

W. Boschin<sup>1,2,3★</sup> and M. Girardi<sup>4,5</sup>

<sup>1</sup>Fundación G. Galilei - INAF (Telescopio Nazionale Galileo), Rambla J. A. Fernández Pérez 7, E-38712 Breña Baja, La Palma, Spain

<sup>2</sup>Instituto de Astrofísica de Canarias, C/Vía Láctea s/n, E-38205 La Laguna, Spain

<sup>3</sup>Departamento de Astrofísica, Universidad de La Laguna, Av. del Astrofísico Francisco Sánchez s/n, E-38205 La Laguna, Spain

<sup>4</sup>Dipartimento di Fisica dell'Università degli Studi di Trieste - Sezione di Astronomia, via Tiepolo 11, I-34143 Trieste, Italy

<sup>5</sup>INAF - Osservatorio Astronomico di Trieste, via Tiepolo 11, I-34143 Trieste, Italy

Accepted 2018 July 9. Received 2018 July 9; in original form 2018 May 28

## ABSTRACT

We present the study of the dynamical status of the galaxy cluster CL1821+643, a rare and intriguing cool-core cluster hosting a giant radio halo. We base our analysis on new spectroscopic data for 129 galaxies acquired at the Italian Telescopio Nazionale *Galileo*. We also use spectroscopic data available from the literature and photometric data from the Sloan Digital Sky Survey. We select 120 cluster member galaxies and compute the cluster redshift ( $z$ )  $\sim 0.296$  and the global line-of-sight velocity dispersion  $\sigma_v \sim 1100 \text{ km s}^{-1}$ . The results of our analysis are consistent with CL1821+643 being a massive ( $M > 10^{15} M_\odot$ ) dynamically relaxed cluster dominated by a big and luminous elliptical at the centre of the cluster potential well. None of the tests employed to study the cluster galaxies kinematics in the 1D (velocity information), 2D (spatial information), and 3D (combined velocity and spatial information) domains is able to detect significant substructures. While this picture is in agreement with previous results based on X-ray data and on the existence of the central cool core, we do not find any evidence of a merging process responsible for the radio halo discovered in this cluster. Thus, this radio halo remains an open problem that raises doubts about our understanding of diffuse radio sources in clusters.

**Key words:** galaxies: clusters: general – galaxies: clusters: individual: CL1821+643 – galaxies: kinematics and dynamics.

## 1 INTRODUCTION

A fraction of the most massive galaxy clusters exhibits in their inner regions diffuse radio sources named *radio haloes* (also *giant radio haloes*, or GRHs). They are extended (on 1 Mpc scales) unpolarized synchrotron sources produced by relativistic electrons and large-scale magnetic fields spread out the intracluster medium (ICM), not associated with compact radio sources like radio galaxies (see e.g. Ferretti et al. 2012 for a review).

The existence of GRHs indicates the presence in the ICM of particle acceleration mechanisms. In particular, GRHs are probably related to turbulence induced in the ICM by recent mergers (e.g. Brunetti & Jones 2015). In fact, for several decades after their discovery, these sources have always been found in dynamically disturbed systems, i.e. massive merging clusters characterized by the absence of a cool core (Ferretti et al. 2012 and references therein).

This picture has dramatically changed in 2014, when Bonafede et al. (2014, hereafter B14) published the discovery of a GRH in the cool-core cluster CL1821+643. More recently, Sommer et al. (2017) found diffuse radio emission at Mpc scale on two  $z \sim 0.22$  relaxed clusters, Abell 2390 and Abell 2261. Another case is Abell 2142 ( $z \sim 0.09$ ), where Venturi et al. (2017) surprisingly found a GRH despite the fact that its optical and X-ray properties do not reveal a major merger. Finally, Savini et al. (2018) reported the detection of diffuse radio emission on scales larger than the core in the cool-core cluster PSZ1G139.61+24 ( $z \sim 0.27$ ).

In summary, these recent findings suggest the possible existence of a new class of dynamically relaxed clusters with GRHs. In the framework of turbulent models this is surprising and challenges the idea that major mergers, necessary to power GRHs, always disrupt the cool core.

In this paper, we focus on one of the puzzling clusters cited above: CL1821+643 (hereafter CL1821). CL1821 hosts an extended central diffuse emission with linear size  $\sim 1.1 h_{70}^{-1} \text{ Mpc}$  and an extrapolated radio power  $P_{1.4\text{GHz}} \sim (3.6\text{--}3.8) 10^{24} \text{ W Hz}^{-1}$  elongated along the SE–NW direction (see B14). Because of its location and size, B14 classified this source as a GRH.

\* E-mail: boschin@tng.iac.es

From the optical point of view, CL1821 (at  $z \sim 0.299$ , Schneider et al. 1992) is dominated by the central quasar H1821+643 (e.g. Hutchings & Neff 1991; Aravena et al. 2011; Reynolds et al. 2014; Walker et al. 2014), an uncommon example of an optically very luminous quasar hosted by the central dominant elliptical galaxy of a massive cluster (see Fig. 1). Moreover, CL1821 appears slightly elongated in the SE–NW direction, as inferred from its weak lensing properties (Wold et al. 2002). However, our present knowledge on this cluster is mainly based on X-ray data. Russell et al. (2010) analysed *Chandra* data taken with the ACIS-S instrument to study the ICM properties. In particular, they found that the ICM temperature drops from  $\sim 9$  to  $\sim 1$  keV, with a short central cooling time of  $\sim 1$  Gyr typical of a relaxed strong cool-core cluster. They also concluded that the quasar did not have a strong impact on the large-scale ICM properties.

The ACIS-S images suggest a projected morphology elongated on the SE–NW direction (a feature revealed also by radio and weak lensing data, see above and Fig. 1) but do not show any evidence of a major merger in this cluster similar to those detected in other clusters with GRHs. Moreover, an analysis of CL1821 based on classical X-ray morphological estimators (concentration parameter  $c$  and power ratio  $P_3/P_0$ ; see B14 and references therein) also supports the hypothesis that it is a relaxed galaxy system. Only the estimator  $w$  (centroid shift parameter), could suggest the existence of an undergoing minor or off-axis merger (see B14).

A more recent work by Kale and Parekh (2016) partially disagrees with the findings of B14, claiming that a morphological analysis of the same *Chandra* data (based on the parameters Gini,  $M_{20}$ , and  $c$ ; see Parekh et al. 2015) puts CL1821 in the category of relaxed/non-relaxed clusters when H1821+643 is included/excluded in/from the analysis.

Nevertheless, the X-ray morphological indicators cited above are not sensitive to eventual mergers along the line of sight (LOS). The only way to explore this possibility and to finally assess the dynamical status of this intriguing cluster is to perform spectroscopic observations of the cluster member galaxies. In fact, the spatial and kinematical analysis of member galaxies constitute an effective tool to detect substructures in clusters and highlight eventual pre-merging subgroups or merger remnants (e.g. Boschin et al. 2004; Boschin, Girardi & Barrena 2013). The optical information complements the results of X-ray studies, also considering that the collisional and non-collisional components of clusters (ICM and galaxies, respectively) exhibit different behaviours during mergers (see e.g. simulations by Roettiger, Loken & Burns 1997).

At the moment only a few dozen of galaxies have known redshifts in an area 30 arcmin wide around H1821+643. Therefore, we decided to perform a spectroscopic survey of CL1821, mainly sampling the central  $\sim 1$  Mpc size region of the cluster characterized by the diffuse X-ray and radio emissions. In particular, we obtained new spectroscopic data at the Italian Telescopio Nazionale *Galileo* (TNG), whose facilities are well suited for the study of a galaxy cluster at  $z \sim 0.3$  like CL1821 (see e.g. the DARC project, Girardi et al. 2011 and references therein<sup>1</sup>).

This paper is organized as follows. We describe the optical observations and present our spectroscopic data catalogue in Section 2. In Section 3 we explain the results of our analysis of the cluster

structure. We discuss our results and present the conclusions in Section 4.

Throughout this paper, we use  $H_0 = 70 \text{ km s}^{-1} \text{ Mpc}^{-1}$  and  $h_{70} = H_0/(70 \text{ km s}^{-1} \text{ Mpc}^{-1})$  in a flat cosmology with  $\Omega_0 = 0.3$  and  $\Omega_\Lambda = 0.7$ . In the adopted cosmology, 1 arcmin corresponds to  $\sim 265 h_{70}^{-1}$  kpc at the cluster redshift. Unless otherwise stated, we indicate errors at the 68 per cent confidence level (hereafter c.l.).

## 2 OBSERVATIONS AND BUILDING OF THE GALAXY CATALOGUE

### 2.1 TNG optical observations

We used the instrument DOLORES of the TNG to perform multi-object spectroscopic (MOS) observations of CL1821 in 2016 June (program CAT16A\_15). In particular, we observed four MOS masks with the LR-B Grism<sup>2</sup> obtaining spectra for 155 objects. The total exposure times were 5400 s for three masks and 3600 s for the last one.

We reduced the spectra with standard IRAF<sup>3</sup> tasks and were able to compute redshifts for 123 galaxies by using the classic cross-correlation technique (Tonry & Davis 1979). For another six galaxies (IDs. 11, 31, 67, 72, 113, and 180, see Table 1), we estimated the redshifts by measuring the wavelength location of prominent emission lines in their spectra (see details of the redshift computation and their errors in Boschin et al. 2013).

### 2.2 Spectroscopic catalogue and prominent galaxies

We also explored the NASA/IPAC Extragalactic Database (NED)<sup>4</sup> to search for galaxies with known redshift lying in the field covered by our spectroscopic survey. In total, we found a set of 72 galaxies with measured redshift. 14 of these galaxies are in common with our TNG data. Since there is no evidence of systematic deviations between these 14 literature redshifts and our measurements, we added the remaining 58 NED galaxies to our sample.

Our final spectroscopic catalogue includes 187 galaxies in the field of CL1821. For all the galaxies, we also use photometric information from the Sloan Digital Sky Survey (SDSS) DR13 in the magnitude bands  $r'$  and  $i'$ .

Table 1 lists the velocity catalogue (see also Fig. 2): identification number of each galaxy, ID (Column 1); equatorial coordinates right ascension and declination,  $\alpha$  and  $\delta$  (J2000, Column 2); (dereddened) SDSS  $r'$  magnitude (Column 3); heliocentric radial velocities,  $V = cz$  (Column 4) with errors;  $\Delta V$  (Column 5).

The cluster galaxy population is dominated by the quasar H1821+643 (ID 94 and hereafter BCG; see its optical spectrum in Fig. 1). Although classified as a radio-quiet quasar, the BCG is a Fanaroff–Riley type I source (Blundell & Rawlings 2001), and is evident in high-resolution radio images of CL1821 taken by B14 (see their fig. 1) and at X-ray wavelengths. ID 85 is the second brightest cluster member in our catalogue and is also an FR–I

<sup>2</sup><http://www.tng.iac.es/instruments/lrs>

<sup>3</sup>IRAF is distributed by the National Optical Astronomy Observatories, which are operated by the Association of Universities for Research in Astronomy, Inc., under cooperative agreement with the National Science Foundation.

<sup>4</sup>NASA/IPAC Extragalactic Database is operated by the Jet Propulsion Laboratory, California Institute of Technology, under contract with the National Aeronautics and Space Administration.

<sup>1</sup>see also <http://www.user.oats.inaf.it/girardi/darc>, the web site of the DARC project.

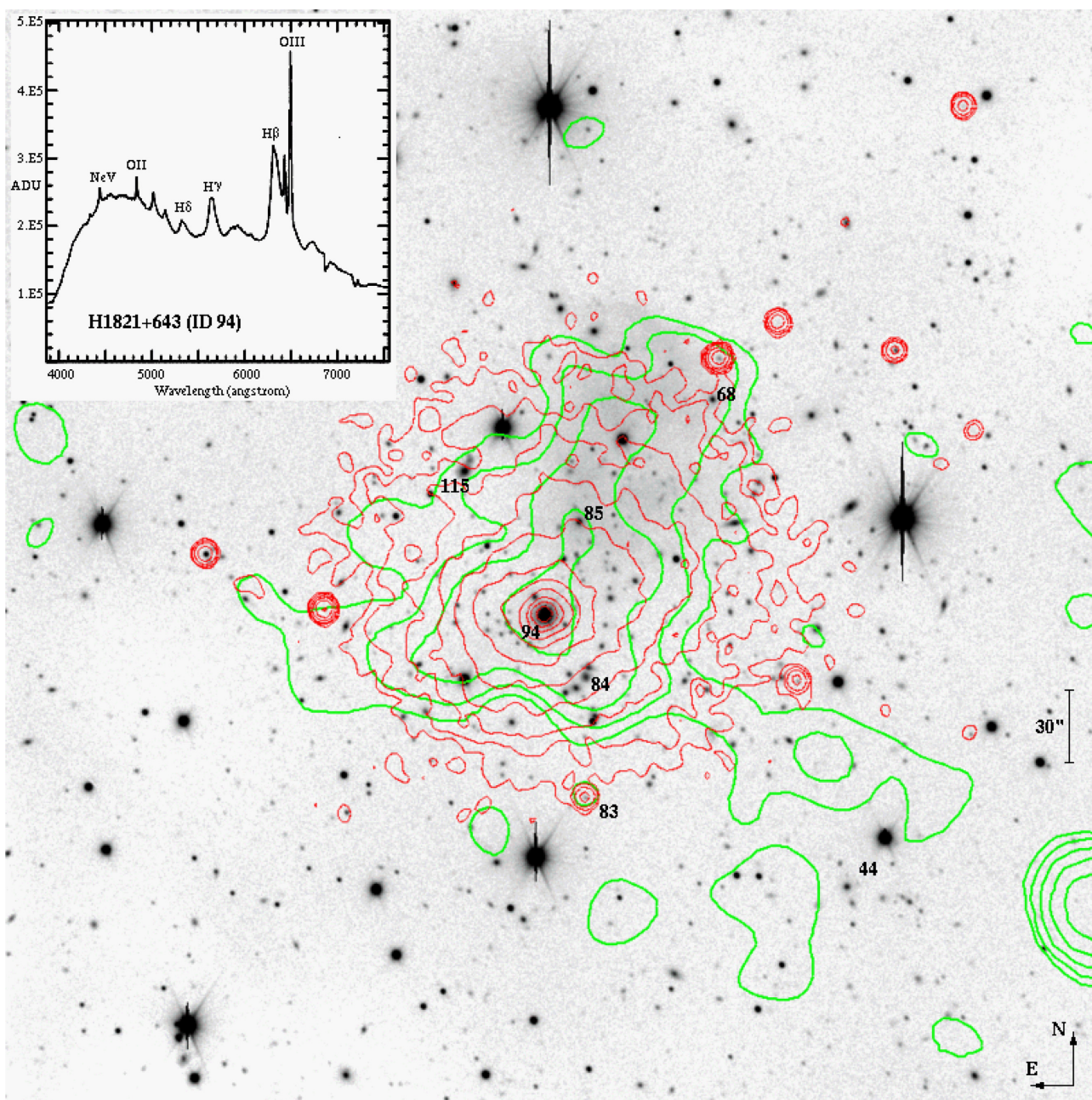


**Figure 1.** The cluster CL1821 in the optical, X-ray, and radio bands. The TNG grey-scale image (FOV  $\sim 8$  arcmin  $\times 8$  arcmin) in the background corresponds to the optical  $r'$ -band. Red thin contours show the cluster X-ray emission in the 0.5–7 keV band (from *Chandra* archival image ID 9398;  $T_{\text{exp}}$ : 34 ks). Thick green contours are the contour levels of a GMRT 323 MHz low-resolution image and show the radio halo (from B14). Top left-hand inset is the TNG wavelength-calibrated spectrum of the central quasar H1821+643 (ID 94; see Table 1). Other labels indicate galaxies mentioned in the text. The diffuse emission visible in the optical image NW of the galaxy ID 85 is the planetary nebula PN G094.0+27.4.

(head-tail) radio galaxy (Lacy, Rawlings & Hill 1992; Blundell & Rawlings 2001). B14 report a bright and elongated radio source  $\sim 2.9$  arcmin SW of BCG (their source ‘D’), at only  $\sim 3$  arcsec from the member galaxy ID 44, which is the probable optical counterpart. Among other galaxies with radio and/or X-ray emission in the field of CL1821, our galaxy ID 83 is a background active galactic nucleus (AGN) with  $z \sim 0.88$ . Fainter radio sources (from B14) appear associated to our galaxies ID 68 (a cluster member) and 84 and 115 (foreground non-member galaxies).

### 3 ANALYSIS OF THE SAMPLE

#### 3.1 Members selection and global properties

The selection of cluster members was performed using two statistical tools: the 1D adaptive-kernel method (hereafter 1D-DEDICA, Pisani 1993) and the ‘shifting gapper’ method (Fadda et al. 1996). First, we ran 1D-DEDICA on the 187 galaxies of our spectroscopic catalogue and detected CL1821 as a prominent velocity peak at  $z \sim 0.296$  populated by 131 provisional cluster members (see Fig. 3).

**Table 1.** Radial velocities of 187 galaxies in the field of CL1821. † highlights the velocities taken from the literature (see the text). IDs in italics refer to non-member galaxies. Galaxy ID 94 is the BCG.

ID	$\alpha, \delta$ (J2000) (18 <sup>h</sup> , +64 <sup>o</sup> )	$r'$	$V$ (km s <sup>-1</sup> )	$\Delta V$ (km s <sup>-1</sup> )
1	20 31.59, 20 24.1	18.68	†75 389	72
2	20 32.09, 22 19.0	18.84	†83 609	114
3	20 33.26, 22 12.2	19.37	†99 630	40
4	20 43.06, 19 45.9	18.33	†26 771	67
5	20 53.44, 19 36.9	17.80	†33 442	100
6	20 56.88, 27 55.5	17.72	†21 495	27
7	21 06.39, 24 56.5	18.89	73 611	110
8	21 07.52, 22 03.7	19.46	89 599	90
9	21 08.58, 24 50.1	19.70	73 745	90
10	21 13.25, 22 40.8	19.24	56 522	95
11	21 13.80, 29 05.2	21.54	148 779	100
12	21 14.79, 12 15.3	19.95	†55 474	35
13	21 16.22, 28 56.4	20.46	117 818	117
14	21 16.59, 22 34.8	20.13	88 890	106
15	21 17.90, 21 18.8	18.83	†89 248	100
16	21 20.04, 22 56.7	18.89	†87 587	53
17	21 21.15, 21 43.6	20.24	†110 084	100
18	21 21.99, 22 15.9	20.11	88 209	154
19	21 22.38, 21 51.1	19.82	86 861	90
20	21 22.47, 28 29.1	17.33	36 706	55
21	21 22.67, 27 29.9	20.14	79 645	180
22	21 23.90, 21 43.8	21.57	†164 346	100
23	21 24.73, 28 39.5	20.43	146 570	88
24	21 25.39, 29 21.7	21.02	117 742	112
25	21 26.19, 23 06.4	20.29	130 358	108
26	21 27.31, 20 52.7	20.94	89 229	103
27	21 27.41, 12 10.5	19.76	†8250	12
28	21 27.44, 21 55.9	20.36	†89 878	100
29	21 29.79, 27 41.0	20.01	89 915	132
30	21 30.35, 20 41.7	19.48	†87 210	100
31	21 31.09, 28 16.6	21.75	85 853	154
32	21 31.93, 17 58.5	20.44	146 525	143
33	21 32.55, 18 32.0	20.02	88 987	99
34	21 32.98, 19 40.7	20.77	88 993	123
35	21 33.17, 20 18.6	20.69	89 495	77
36	21 33.43, 26 03.0	18.88	89 826	84
37	21 34.24, 20 58.2	20.56	†88 918	100
38	21 34.48, 20 30.2	19.84	†87 072	82
39	21 35.39, 25 24.6	18.19	†56 661	100
40	21 36.00, 25 48.2	18.27	56 836	42
41	21 36.37, 19 31.4	20.43	88 725	106
42	21 36.71, 21 24.6	18.21	†51 223	74
43	21 36.73, 25 31.1	18.20	67 816	66
44	21 36.76, 18 38.5	19.06	89 491	66
45	21 37.07, 21 55.8	20.44	85 899	108
46	21 37.07, 23 28.4	19.33	88 842	88
47	21 37.51, 25 23.9	20.38	91 479	101
48	21 37.72, 22 35.0	19.93	85 741	75
49	21 38.00, 27 51.8	18.88	89 440	103
50	21 38.79, 22 57.8	19.69	67 852	79
51	21 38.91, 20 30.9	19.10	†67 903	32
52	21 39.37, 22 04.3	18.82	†86 580	92
53	21 39.57, 15 20.3	18.69	†91 524	50
54	21 39.99, 24 27.7	19.88	90 396	80
55	21 40.02, 24 42.5	19.60	88 670	145
56	21 40.71, 19 42.2	19.56	89 368	88
57	21 41.13, 19 56.6	20.67	86 653	110
58	21 41.25, 23 13.4	20.17	49 290	110
59	21 41.87, 23 24.0	20.65	88 200	167
60	21 42.90, 21 35.0	20.13	86 930	147
61	21 43.18, 21 30.0	20.35	85 307	136

**Table 1** – *continued*

ID	$\alpha, \delta$ (J2000) (18 <sup>h</sup> , +64 <sup>o</sup> )	$r'$	$V$ (km s <sup>-1</sup> )	$\Delta V$ (km s <sup>-1</sup> )
62	21 43.37, 21 05.0	19.53	88 883	103
63	21 43.71, 24 04.0	20.20	88 092	84
64	21 44.46, 21 17.2	18.76	89 154	59
65	21 44.69, 25 13.3	19.78	88 496	130
66	21 44.86, 24 11.1	18.57	87 976	79
67	21 45.33, 17 49.2	20.72	153 152	121
68	21 46.02, 22 11.1	19.01	89 467	75
69	21 47.71, 22 55.1	20.00	87 825	114
70	21 47.78, 20 07.9	19.89	†87 539	100
71	21 48.33, 18 00.0	18.93	89 988	88
72	21 48.41, 17 01.2	20.77	56 519	143
73	21 48.75, 24 20.3	19.55	86 423	88
74	21 49.54, 21 03.1	20.40	89 747	88
75	21 50.10, 19 22.7	20.16	87 940	238
76	21 50.58, 17 11.4	20.04	89 298	90
77	21 51.16, 20 51.5	20.04	†88 079	100
78	21 52.82, 20 43.9	19.71	†90 387	300
79	21 53.14, 20 32.0	21.16	†119 917	300
80	21 53.36, 20 23.0	20.22	†87 108	83
81	21 54.06, 22 40.5	18.46	53 682	97
82	21 54.25, 20 13.7	19.70	†89 788	300
83	21 54.34, 19 16.6	22.23	262 551	394
84	21 54.44, 20 09.6	19.11	†67 633	150
85	21 54.96, 21 17.2	18.23	†91 137	300
86	21 55.09, 20 04.8	19.36	†87 839	100
87	21 55.20, 23 41.2	20.38	88 807	158
88	21 55.56, 20 10.4	20.19	89 103	114
89	21 55.80, 20 02.7	19.69	†90 819	55
90	21 56.00, 21 00.9	19.22	†87 419	150
91	21 56.35, 22 50.2	18.94	†73 254	64
92	21 56.92, 22 55.9	19.82	73 731	44
93	21 57.10, 22 29.4	20.67	91 369	125
94	21 57.24, 20 36.2	13.60	89 054	48
95	21 57.86, 20 44.2	19.79	†90 327	100
96	21 58.06, 23 16.2	20.34	90 691	119
97	21 58.26, 20 23.3	19.98	88 271	130
98	21 58.53, 18 23.3	19.61	†87 288	89
99	21 58.73, 26 44.2	19.62	†88 595	84
100	21 58.83, 24 03.2	20.96	90 203	132
101	21 58.86, 23 08.4	19.36	91 283	84
102	21 59.35, 23 29.2	20.20	88 972	136
103	21 59.41, 19 49.3	19.48	†88 289	300
104	21 59.99, 19 31.2	20.84	86 866	117
105	22 00.02, 19 26.2	21.44	89 579	114
106	22 00.35, 22 41.6	20.75	91 662	139
107	22 00.36, 18 48.1	19.04	86 260	59
108	22 01.09, 20 29.6	21.21	†88 439	100
109	22 01.13, 17 00.6	21.16	80 169	121
110	22 01.21, 17 02.5	19.63	79 486	136
111	22 01.48, 28 03.7	21.55	178 877	108
112	22 02.14, 19 03.4	20.27	89 787	95
113	22 02.40, 21 43.7	19.75	89 200	103
114	22 02.69, 27 13.7	19.20	89 219	121
115	22 02.71, 21 38.9	18.10	36 368	86
116	22 02.85, 26 44.5	20.71	89 022	150
117	22 03.13, 20 40.3	20.37	88 322	114
118	22 03.26, 20 32.6	20.36	91 075	66
119	22 03.53, 23 00.9	18.57	†89 236	80
120	22 03.63, 24 45.3	19.64	87 826	81
121	22 03.95, 22 20.0	19.93	85 679	53
122	22 04.55, 20 53.5	20.77	†85 261	100
123	22 04.96, 21 48.6	20.56	89 694	103
124	22 05.23, 19 53.9	19.99	88 874	101

Table 1 – continued

ID	$\alpha, \delta$ (J2000)	$r'$	$V$	$\Delta V$
	(18 <sup>h</sup> , +64 <sup>o</sup> )		(km s <sup>-1</sup> )	(km s <sup>-1</sup> )
125	22 06.20, 24 14.1	20.60	89 703	163
126	22 06.72, 19 51.4	19.94	†90 477	100
127	22 07.44, 24 14.0	20.82	86 153	154
128	22 07.57, 26 14.3	20.75	90 618	95
129	22 07.86, 21 50.6	20.33	90 209	88
130	22 08.15, 18 45.5	21.13	87 170	141
131	22 09.19, 17 34.7	20.08	86 584	66
132	22 10.36, 17 14.8	18.49	†79 952	80
133	22 10.63, 20 30.7	19.01	†87 449	100
134	22 10.98, 20 49.8	19.65	86 298	59
135	22 11.19, 21 20.4	19.55	90 179	101
136	22 11.33, 28 50.3	19.81	†99 138	144
137	22 12.33, 20 07.9	19.68	88 022	68
138	22 12.41, 22 10.9	20.63	88 765	169
139	22 12.62, 26 31.4	18.67	†89 422	66
140	22 13.67, 20 16.5	20.89	†89 008	100
141	22 13.79, 18 11.3	20.51	87 989	134
142	22 17.42, 20 42.3	19.76	†89 938	100
143	22 19.21, 18 43.1	20.18	†73 653	86
144	22 19.93, 23 34.7	19.27	87 897	51
145	22 19.97, 21 49.4	20.50	†53 513	100
146	22 20.59, 18 20.8	20.19	155 238	134
147	22 20.96, 26 51.0	16.64	†57 596	35
148	22 21.24, 17 21.1	19.43	87 092	150
149	22 21.39, 13 33.7	21.67	126 279	90
150	22 21.94, 21 26.4	20.11	89 185	62
151	22 25.21, 22 44.9	19.52	†56 862	40
152	22 26.95, 15 35.4	20.36	89 798	136
153	22 27.37, 18 19.6	19.94	88 821	121
154	22 28.22, 20 43.2	19.96	†88 529	100
155	22 29.75, 23 08.2	18.05	†57 446	53
156	22 30.13, 13 15.6	18.89	†83 903	55
157	22 30.35, 20 01.9	20.03	90 509	92
158	22 31.94, 19 39.0	19.74	†90 238	100
159	22 32.36, 14 38.2	20.00	88 410	125
160	22 32.61, 12 45.2	20.39	84 424	233
161	22 32.88, 18 22.0	20.09	73 594	141
162	22 33.20, 18 50.4	19.68	†88 382	54
163	22 33.21, 14 32.9	19.71	90 483	114
164	22 34.61, 20 55.9	20.07	†90 238	100
165	22 35.63, 18 59.8	20.38	89 943	123
166	22 35.70, 16 40.7	19.47	90 309	123
167	22 36.39, 14 49.6	20.11	87 349	128
168	22 40.09, 19 21.2	19.45	87 967	88
169	22 41.06, 19 53.2	20.59	90 338	75
170	22 41.16, 14 59.8	19.02	57 626	75
171	22 41.21, 18 52.0	20.53	89 142	108
172	22 42.50, 17 15.1	19.55	72 691	84
173	22 43.12, 13 19.0	20.09	84 216	106
174	22 43.89, 16 24.1	19.95	130 560	123
175	22 48.41, 17 59.5	21.96	224 389	103
176	22 49.09, 14 11.6	19.60	80 114	84
177	22 49.60, 19 44.4	20.12	90 348	95
178	22 49.63, 16 06.9	19.97	82 326	123
179	22 49.85, 19 28.1	18.93	49 129	88
180	22 52.49, 17 38.7	21.49	167 915	157
181	22 55.75, 14 01.7	19.31	89 898	128
182	22 57.06, 15 07.6	20.92	110 810	114
183	23 02.99, 13 46.2	20.93	78 316	163
184	23 03.60, 13 01.2	20.40	65 097	86
185	23 06.64, 18 09.9	21.01	88 598	161
186	23 16.49, 17 22.6	20.11	147 851	156
187	23 19.29, 19 31.0	18.30	†172 860	300

In the second step, we combined the spatial and velocity information for the provisional members by running the ‘shifting gapper’ test. In particular, we chose a gap of 1000 km s<sup>-1</sup> (see also Girardi et al. 1996) and adopted for the cluster centre the location of the BCG. With this tool we rejected another 11 galaxies leading to a final sample of 120 cluster members, whose projected phase space is shown in Fig. 4.

The velocity distribution of the 120 cluster members was analysed with the biweight routines by Beers, Flynn, and Gebhardt (1990), which provide robust estimates of location and scale. Our measurement of the mean cluster redshift is  $\langle z \rangle = 0.2965 \pm 0.0003$  (i.e.  $\langle V \rangle = 88\,878 \pm 104$  km s<sup>-1</sup>). Instead, the global LOS velocity dispersion is  $\sigma_V = 1137_{-78}^{+72}$  km s<sup>-1</sup>. Adopting the  $\sigma_V$ – $M_{200}$  relation of Munari et al. (2013; derived from cosmological  $N$ -body and hydrodynamic simulations in the  $\Lambda$ -cold dark matter framework), we compute a total cluster mass of  $M_{200} = (1.4 \pm 0.2) \times 10^{15} M_{\odot}$  within  $R_{200} = 2.1$  Mpc.

### 3.2 Cluster substructures

We searched for substructures by using 1D (velocity information), 2D (spatial distribution), and 3D (combined velocity and spatial information) statistical tests.

The 1D analysis consists of a detailed study of the properties of the velocity distribution of member galaxies (Fig. 3). In particular, we do not find significant evidence of deviations from Gaussianity (a possible hint of complex dynamics in the cluster) according to several parameters (kurtosis, skewness, and tail index). Instead, there is marginal evidence of asymmetry according to the W-Test ( $\sim 95$  per cent c.l.) and the asymmetry index ( $\sim 90$ – $95$  per cent c.l.; see Bird & Beers 1993 for details).

We also run the 1D-Kaye Mixture Model test (1D-KMM; Ashman, Bird & Zepf 1994; see also for recent applications Girardi et al. 2008 and Balestra et al. 2016) to search for bimodal partitions of the velocity distribution fitting the data better than a single Gaussian. In the homoscedastic case (i.e. assuming equal velocity dispersions), the most likely solution (at the 95 per cent c.l.) identifies two peaks at 87 124 and 89 428 km s<sup>-1</sup> with  $\sigma_V \sim 800 \pm 100$  km s<sup>-1</sup> populated by 29 and 91 galaxies, respectively. According to the 2D Kolmogorov–Smirnov test, it is not possible to separate the two peaks in the spatial domain. Instead, in the physically more realistic (heteroscedastic, i.e. assuming different velocity dispersions) case, the 1D-KMM test does not provide any significant solution.

About the analysis of the 2D spatial distribution of the spectroscopic member galaxies, we employed the 2D adaptive-kernel method of Pisani et al. (1996, hereafter 2D-DEDICA). The results are shown in Fig. 5. This test detects CL1821 as a very prominent galaxy peak with two low-density secondary clumps: the densest one is located  $\sim 2$  arcmin N of the cluster centre (density only  $\sim 35$  per cent the main peak) and the second one lies  $\sim 4$  arcmin ESE of the cluster centre (see also Table 2). However, the existence of these two low-density subclumps appears very questionable, also taking into account that our spectroscopic data do not cover the entire cluster field and are affected by magnitude incompleteness due to unavoidable constraints in the design of the MOS masks.

We can overcome our incompleteness problems by using the SDSS photometry of the cluster field at our disposal. In particular, we consider all the galaxies within 3 Mpc from the cluster centre and select likely members on the basis of the ( $r' - i'$  versus  $r'$ ) colour-magnitude relation (hereafter CMR), which allows to identify the locus of the dominant cluster population (i.e. early-type galaxies, Dressler 1980). We determine the CMR by applying the

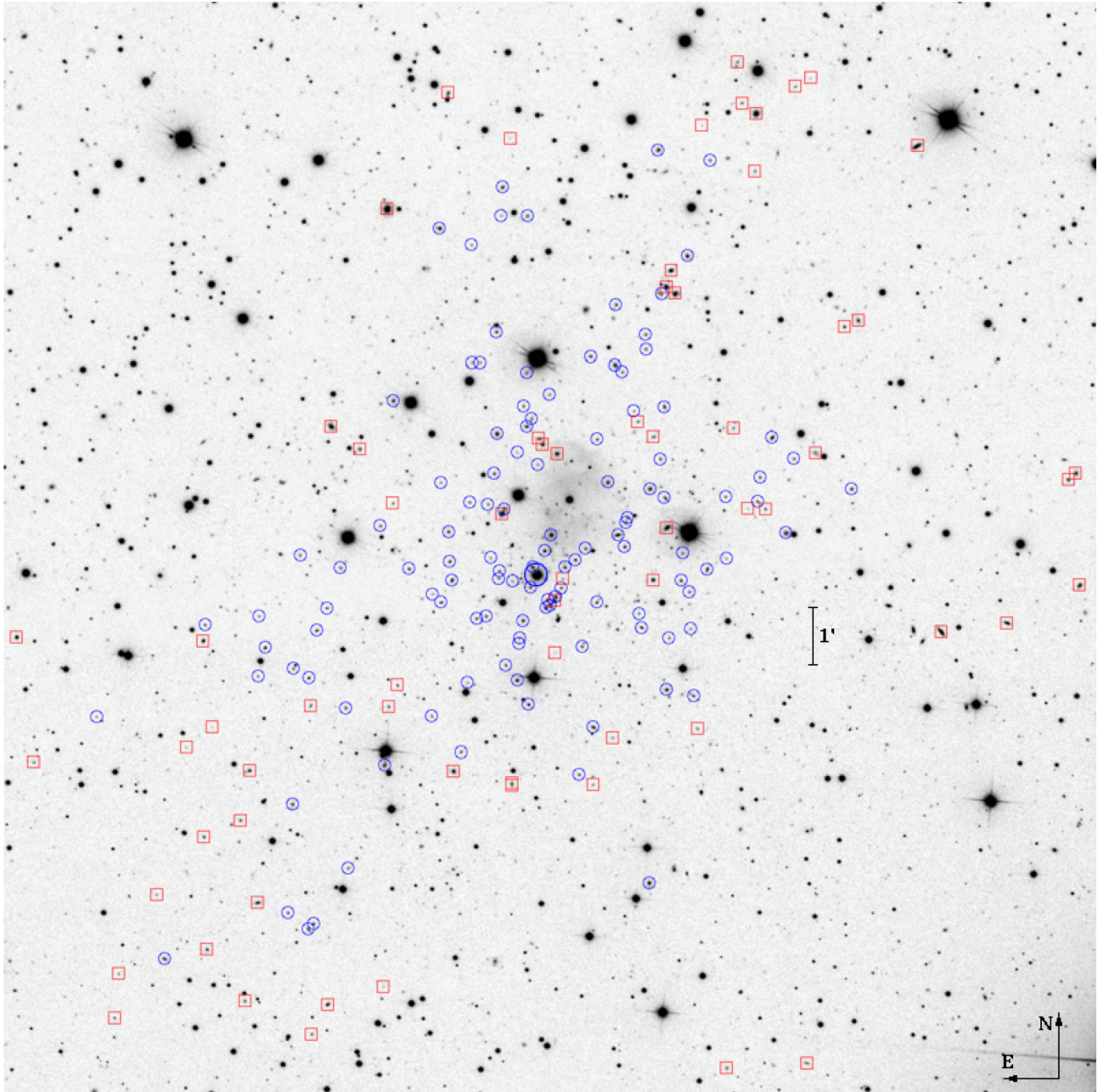
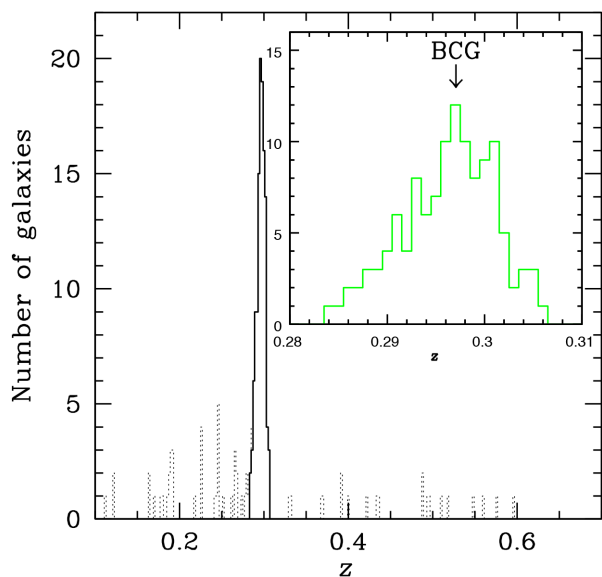


**Figure 2.** Wide field SDSS image (filter  $r'$ ) of the cluster CL1821 showing the positions of the galaxies of our spectroscopic catalogue. Blue circles and red squares indicate cluster members and non-member galaxies, respectively (see Table 1). The biggest circle in the centre highlights the central quasar H1821+643 (ID 94 and BCG; see the text).

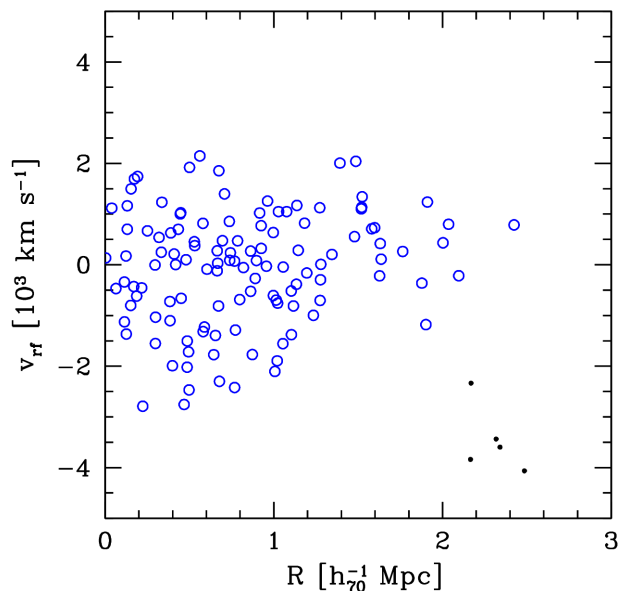
$2\sigma$ -clipping fitting procedure to the cluster members and obtain  $r' - i' = 1.093 - 0.028 \times r'$  (see Fig. 6). Then, within the photometric catalogue we consider as likely ‘red’ cluster members, the galaxies with colour index within 0.16 mag of the CMR (i.e. the  $1\sigma$ -error associated to the fitted intercept).

Fig. 7 shows the contour map for the 508 likely cluster members having  $r' \leq 21$ , according to 2D-DEDICA. There is no trace now of the two subclumps found with the previous analysis, thus suggesting that they are artefacts due to the incompleteness of the spectroscopic sample. Instead, there is evidence of a more distant subgroup lying  $\sim 2$  Mpc ( $\sim R_{200}$ ) NNE of the cluster centre (see Table 3).

The existence of this external structure is also confirmed by the Voronoi Tessellation and Percolation (VTP) technique (e.g. Ramella et al. 2001; Barrena et al. 2005), a non-parametric test, which is sensitive to galaxy structures regardless of their shapes. Considering again the 508 likely members with  $r' \leq 21$ , we run VTP over this set four times adopting four detection thresholds. The results are shown in Fig. 8, where galaxies identified as belonging to structures at 90, 95, 98, and 99 per cent c.l.s. are drawn as open squares, crosses, triangles, and solid circles, respectively. Once again VTP detects the main body of CL1821 without hints of substructures and the new external group at NNE, even though the last one is at the lowest c.l.



**Figure 3.** Redshift galaxy distribution. The heavy line histogram refers to the 131 galaxies assigned to CL1821 according to the 1D-DEDICA reconstruction method. The inset figure shows the member-galaxy distribution (after final selection with the ‘shifting gapper’ method) with the indication of the BCG redshift.



**Figure 4.** Rest-frame velocity versus projected cluster-centric distance for the 120 member galaxies (blue circles). Black dots are galaxies selected by 1D-DEDICA but rejected by the ‘shifting gapper’ test.

As for the 3D analysis, we employed different tools to search for a correlation between velocity and position information, which would be a clear sign of real substructures in the cluster.

First, we find no evidence of a significant velocity gradient (see e.g. den Hartog & Katgert 1996 and Girardi et al. 1996 for the details of the method) in the sample of the 120 spectroscopic cluster members.

Then, over the same sample we apply the classical  $\Delta$ -test (Dressler & Schectman 1988, hereafter DS test), which is considered as the most sensitive 3D test (e.g. Pinkney et al. 1996). For each spectroscopic member galaxy, the DS test computes the deviation

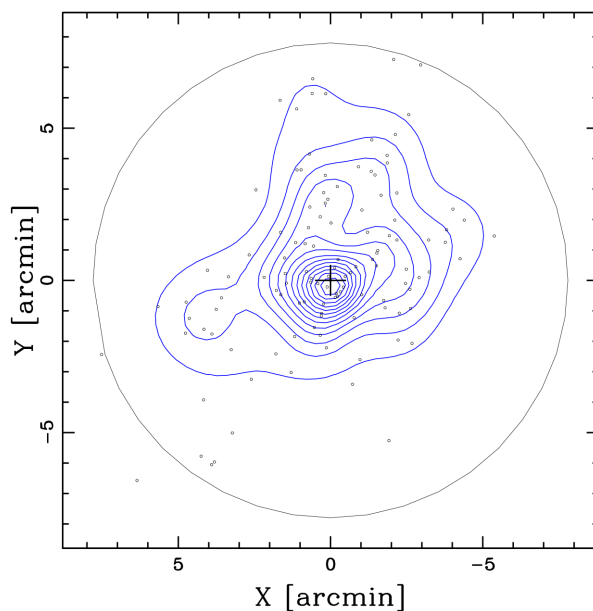


**Figure 5.** Spatial distribution on the sky of the 120 spectroscopic cluster members and relative isodensity contour map obtained with the 2D-DEDICA method. The black cross indicates the position of BCG. The plot is centred on the cluster centre and circle contains the cluster within a radius equal to 7.8 arcmin  $\sim 2.1 h_{70}^{-1}$  Mpc ( $\sim R_{200}$ ).

**Table 2.** The 2D structure of CL1821. Results from the spectroscopic sample according to the 2D-DEDICA method. For each subclump the table lists the number of assigned member galaxies  $N_S$ , equatorial coordinates of the density peak, the relative density with respect to the highest peak  $\rho_S$ , and the  $\chi^2$  value of the peak.

Subclump	$N_S$	$\alpha(J2000), \delta(J2000)$ h : m : s. ° : ' : ''	$\rho_S$	$\chi_S^2$
C	72	18 21 57.1,+64 20 25	1.00	33.3
N	30	18 21 59.2,+64 23 01	0.35	12.8
ESE	13	18 22 34.5,+64 19 24	0.17	6.2

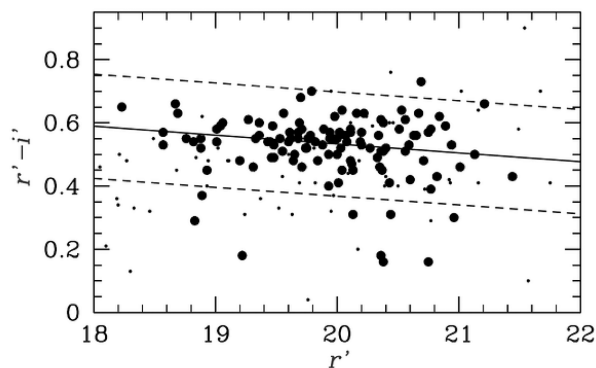


**Figure 6.**  $r' - i'$  versus  $r'$  diagram for galaxies with available spectroscopy. Big circles and dots indicate member and non-member galaxies, respectively. The solid line gives the CMR determined on member galaxies; the dashed lines are drawn at colour index  $\pm 0.16$  mag from the CMR (see the text).

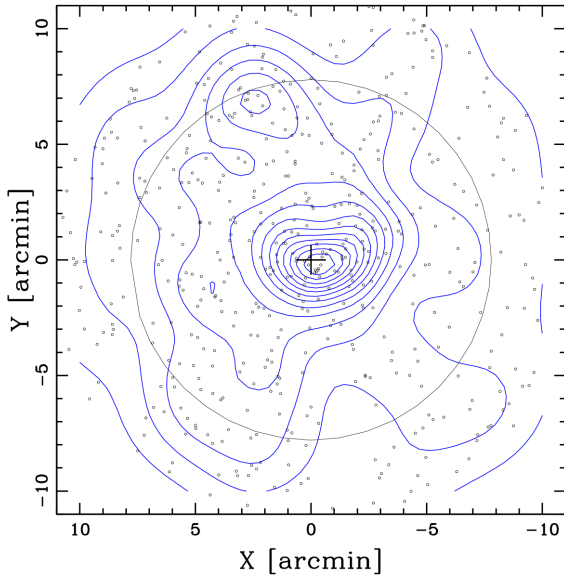


**Figure 7.** Spatial distribution on the sky and relative isodensity contour map of the photometric likely cluster members with  $r' \leq 21$  obtained with the 2D-DEDICA test. The plot is centred on the cluster centre and circle contains the cluster within a radius equal to 7.8 arcmin  $\sim 2.1 h_{70}^{-1}$  Mpc ( $\sim R_{200}$ ).

**Table 3.** The 2D structure of CL1821. Results from the sample of photometric likely members according to the 2D-DEDICA method. For each subclump the table lists the number of assigned member galaxies  $N_S$ , equatorial coordinates of the density peak, the relative density with respect to the highest peak  $\rho_S$ , and the  $\chi^2$  value of the peak.

Subclump	$N_S$	$\alpha(\text{J2000}), \delta(\text{J2000})$ h : m : s, ° : ' : ''	$\rho_S$	$\chi^2_S$
C	330	18 21 54.3,+64 20 24	1.00	50.3
NNE	67	18 22 20.0,+64 27 28	0.45	16.8

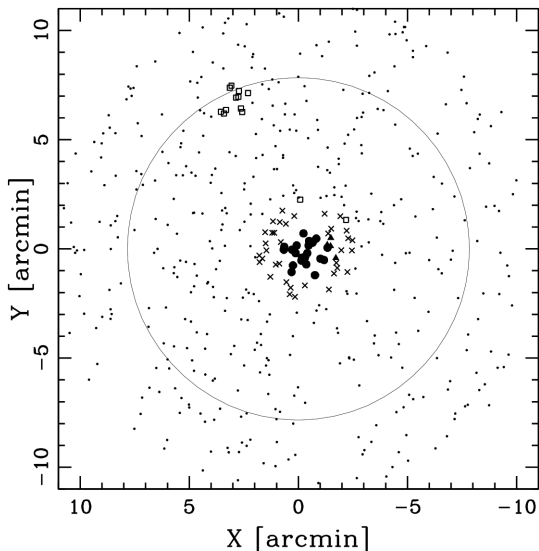


**Figure 8.** Galaxies belonging to structures as detected by the VTP method. The algorithm is run on the sample of likely members with  $r' \leq 21$  (see the text). Open squares, crosses, triangles, and solid circles indicate galaxies in structures at the 90, 95, 98, and 99 per cent c.l.s., respectively. The plot is centred on the cluster centre and circle contains the cluster within a radius equal to 7.8 arcmin  $\sim 2.1 h_{70}^{-1}$  Mpc ( $\sim R_{200}$ ).

$\delta$  defined as  $\delta^2 = \delta_V^2 + \delta_S^2$ , where  $\delta_V^2 = [(N_{\text{nn}} + 1)/\sigma_V^2] \times (\overline{V}_{\text{loc}} - \overline{V})^2$ ,  $\delta_S^2 = [(N_{\text{nn}} + 1)/\sigma_V^2] \times (\sigma_{V,\text{loc}} - \sigma_V)^2$  and the subscript ‘loc’ denotes the local quantities computed over the set containing the galaxy and its  $N_{\text{nn}} = 10$  neighbours. The parameter  $\Delta$  is then defined as the sum of the  $\delta$  of the individual galaxies and provides the cumulative deviation of the local kinematical parameters (mean velocity and velocity dispersion) from the global cluster parameters. The significance of  $\Delta$ , i.e. of substructure, is finally checked by running Monte Carlo simulations.

No significant substructure is found in CL1821 with the DS test and its modified versions, which consider separately the local mean velocity (parameter  $\delta_V^2$ ) and velocity dispersion (parameter  $\delta_S^2$ ) as kinematical indicators (see Girardi, Boschin & Barrena 2010).

Finally, we resorted to the hierarchical tree (Htree) algorithm developed by Serna and Gerbal (1996; see also Girardi et al. 2011 and Durret et al. 2015 for recent applications). We apply it to the catalogue of 120 member galaxies with known radial velocities and  $r'$ -band magnitudes. The method executes a hierarchical clustering analysis and extracts galaxy subgroups by computing the relative binding energies of member galaxies. It has proved to be effective to detect substructures both in nearby clusters (e.g. Coma – Adami et al. 2005) and in medium-redshift clusters (e.g. Abell 1995 – Boschin et al. 2012a). It works with a constant value for the mass-to-light ratio of galaxies. Here we adopt a value of  $M/L_{r'} = 150 h_{70} M_{\odot}/L_{\odot}$  (a value comparable to that of clusters, see Serna & Gerbal 1996), but the gross results are quite robust against the choice of the value of  $M/L_{r'}$ . We also assume a magnitude  $r' \sim +17$  for the host galaxy (the BCG) of the central quasar H1821+643 (from measurements performed by Hutchings and Neff 1991 and Floyd et al. 2004) and choose  $n = 10$  as the minimum number of galaxies in substructures (e.g. Durret et al. 2015). The Htree method does not find significant substructure in CL1821.

#### 4 DISCUSSION AND CONCLUSIONS

The high values of the velocity dispersion  $\sigma_V = 1137_{-78}^{+72}$  km s $^{-1}$  and X-ray temperature  $kT_X = (9.0 \pm 0.5)$  keV (excluding the central cool core; Russell et al. 2010) of CL1821 are typical of hot, massive clusters (e.g. Girardi & Mezzetti 2001). Moreover, our estimate of  $\sigma_V$  and  $T_X$  are consistent with each other under the assumption of energy density equipartition between ICM and galaxies. In fact, we obtain  $\beta_{\text{spec}} = \sigma_V^2/(kT_X/\mu m_p) = 0.87_{-0.12}^{+0.13}$ , to be compared with  $\beta_{\text{spec}} = 1$ .<sup>5</sup> This differs from what is commonly found in merging clusters hosting GRHs, where values of  $\beta_{\text{spec}}$  significantly greater than unity are often found (e.g. Abell 2744 – Boschin et al. 2006; Abell 2254 – Girardi et al. 2011; Abell 1758N – Boschin et al. 2012b; Abell 1351 – Barrena et al. 2014).

However, the most convincing evidence that CL1821 is not interested in a major merger comes from the absence of significant substructures, according to the analysis of our optical data.

In particular, the analysis of the 2D galaxy distribution performed with the 2D-DEDICA test detects CL1821 as a very prominent and well- isolated galaxy peak. The only significant subclump is the one located at a projected distance of  $\sim 2$  Mpc NNE of the cluster centre and detected on the sample of ‘likely’ members both with 2D-DEDICA (see Fig. 7 and Table 3) and with the VTP method (Fig. 8). Unfortunately, we have very few redshifts in the region of the subgroup, and its full characterization is not possible. However, its projected galaxy density makes of it a minor system at  $R_{200}$  from

<sup>5</sup> $\mu = 0.58$  is the mean molecular weight and  $m_p$  the proton mass.



the cluster centre, which does not seem able to perturb significantly the potential well of CL1821.

These findings in the spatial domain agree, as expected, with the lack of major substructures observed in *Chandra* X-ray data (B14; Russell et al. 2010). However, our main goal was to explore the existence of ongoing mergers along the LOS. The 1D velocity distribution of member galaxies would provide a decisive contribution in this sense. Our results do not show strong evidence of departure from Gaussianity and asymmetry, which would be important signs of a dynamically perturbed cluster. The 1D-KMM test proposes a marginally significant partition of the velocity distribution in two peaks, but only in the physically (homoscedastic) less realistic case. In the heteroscedastic case, on the contrary, 1D-KMM does not find any significant solution for a bimodal (or more complex) partition of the velocity distribution.

Finally, combining the velocity and position information of member galaxies we do not find evidence of a significant velocity gradient. This suggests that eventual substructures would be mainly LOS aligned, but the results of the DS test and the Htree method agree with the negative findings of the 1D and 2D analysis.

In conclusion, our new optical data provide a picture of CL1821 consistent with being a massive dynamically relaxed cluster dominated by a BCG located in the centre of the cluster both in the velocity (see Fig. 3) and in the spatial domains. According to our results, the presence of a cool core in CL1821 is not surprising, even though a cool core is not necessarily disrupted if a cluster is affected by a merger with enough angular momentum (see e.g. simulations by Poole et al. 2008; Hahn et al. 2017).

Nevertheless, the absence of major substructures within 1.5–2 Mpc from the cluster centre is in conflict with the existence of the GRH discovered in CL1821.

Indeed, a major merger is not always needed to produce diffuse radio emission in a cluster. In fact, minor mergers are also predicted to form haloes with ultrasteep radio spectrum and low-radio power with respect to major mergers (e.g. Cassano, Brunetti & Setti 2006; Brunetti et al. 2008), but leaving the cluster core intact. This could be the case of PSZ1G139.61+24 mentioned in Section 1 (Savini et al. 2018), a cool-core cluster with an associated mini-halo and a low-size ( $\sim 0.5$  Mpc) and underluminous radio halo with a spectral index<sup>6</sup>  $\alpha \gtrsim 1.7$ . However, the GRH hosted by CL1821 and the halo found in PSZ1G139.61+24 can be hardly compared with each other, especially considering that the GRH of CL1821 resembles more a ‘classical’ radio halo, with a flatter spectrum ( $\alpha \sim 1.0$ – $1.1$ ) and a size of  $\gtrsim 1$  Mpc (see B14).

Instead, PSZ1G139.61+24 shares some similarities with Abell 2142, another cluster which is not a major merger but presents a two-component diffuse radio emission (Venturi et al. 2017). Its central brightest component has a spectral index  $\alpha$  similar to those of typical radio haloes, and Venturi et al. (2017) propose that it could be powered by the gas sloshing in the centre of the cluster (similar to the scenario suggested for the formation of radio mini-haloes in cool-core clusters; see e.g. Mazzotta & Giacintucci 2008; ZuHone et al. 2013) with a central AGN activity, which would provide seed electrons then reaccelerated in the ICM. If such a mechanism could play any role in explaining also the GRH of CL1821 is questionable. In fact, in terms of overall size and spectral steepness the GRH of CL1821 could partially resemble the diffuse emission in Abell 2142. Moreover, the central BCG (and perhaps also the second brightest member ID 85; see Section 2.2) could act as the AGNs located in

the centre of Abell 2142. However, the differences between the two clusters are evident – CL1821 is a cool-core cluster, and according to our analysis, does not show obvious signs of recent mergers, while Abell 2142 is not a cool-core cluster and exhibits multiple cold fronts, which are signs of past minor merger activity.

In conclusion, the existence of the GRH hosted by CL1821 remains an open problem, which brings into question our current understanding of cool-core clusters and diffuse radio emission in clusters.

## ACKNOWLEDGEMENTS

We thank the anonymous referee for his/her useful comments and suggestions.

MG acknowledges the support from the grant MIUR PRIN 2015 ‘Cosmology and Fundamental Physics: illuminating the Dark Universe with Euclid’.

This publication is based on observations made on the island of La Palma with the Italian Telescopio Nazionale Galileo (TNG), which is operated by the Fundación Galileo Galilei – INAF (Istituto Nazionale di Astrofisica) and is located in the Spanish Observatorio de the Roque de Los Muchachos of the Instituto de Astrofísica de Canarias.

This research has made use of the galaxy catalogue of the Sloan Digital Sky Survey (SDSS). The SDSS web site is <http://www.sdss.org/>, where the list of the funding organizations and collaborating institutions can be found.

## REFERENCES

- Adami C., Biviano A., Durret F., Mazure A., 2005, *A&A*, 443, 17  
 Aravena M., Wagg J., Papadopoulos P. P., Feain I. J., 2011, *ApJ*, 737, 64  
 Ashman K. M., Bird C. M., Zepf S. E., 1994, *AJ*, 108, 2348  
 Balestra I. et al., 2016, *ApJS*, 224, 33  
 Barrena R., Ramella M., Boschin W., Nonino M., Biviano A., Mediavilla E., 2005, *A&A*, 444, 685  
 Barrena R., Girardi M., Boschin W., De Grandi S., Rossetti M., 2014, *MNRAS*, 442, 2216  
 Beers T. C., Flynn K., Gebhardt K., 1990, *AJ*, 100, 32  
 Bird C. M., Beers T. C., 1993, *AJ*, 105, 1596  
 Blundell K. M., Rawlings S., 2001, *ApJ*, 562, L5  
 Bonafede A. et al., 2014, *MNRAS*, 444, L44 (B14)  
 Boschin W., Girardi M., Barrena R., Biviano A., Feretti L., Ramella M., 2004, *A&A*, 416, 839  
 Boschin W., Girardi M., Spolaor M., Barrena R., 2006, *A&A*, 449, 461  
 Boschin W., Girardi M., Barrena R., 2012a, *A&A*, 547, A44  
 Boschin W., Girardi M., Barrena R., Nonino M., 2012b, *A&A*, 540, A43  
 Boschin W., Girardi M., Barrena R., 2013, *MNRAS*, 434, 772  
 Brunetti G., Jones T. W., 2015, *Astrophysics and Space Science Library*, Vol. 407, *Magnetic Fields in Diffuse Media*. Springer, Berlin, p. 557  
 Brunetti G. et al., 2008, *Nature*, 455, 944  
 Cassano R., Brunetti G., Setti G., 2006, *MNRAS*, 369, 1577  
 den Hartog R., Katgert P., 1996, *MNRAS*, 279, 349  
 Dressler A., 1980, *ApJ*, 236, 351  
 Dressler A., Shectman S. A., 1988, *AJ*, 95, 985  
 Durret F., Wakamatsu K., Nagayama T., Adami C., Biviano A., 2015, *A&A*, 583, A124  
 Fadda D., Girardi M., Giuricin G., Mardirossian F., Mezzetti M., 1996, *ApJ*, 473, 670  
 Feretti L., Giovannini G., Govoni F., Murgia M., 2012, *A&ARv*, 20, 54  
 Floyd D. J. E., Kukula M. J., Dunlop J. S., McLure R. J., Miller L., Percival W. J., Baum S. A., O’Dea C. P., 2004, *MNRAS*, 355, 196  
 Girardi M., Mezzetti M., 2001, *ApJ*, 548, 79  
 Girardi M., Fadda D., Giuricin G., Mardirossian F., Mezzetti M., Biviano A., 1996, *ApJ*, 457, 61

<sup>6</sup>We define the radio spectrum as  $S(\nu) \propto \nu^{-\alpha}$ .

- Girardi M., Barrena R., Boschin W., Ellingson E., 2008, *A&A*, 491, 379
- Girardi M., Boschin W., Barrena R., 2010, *A&A*, 517, A65
- Girardi M., Bardelli S., Barrena R., Boschin W., Gastaldello F., Nonino M., 2011, *A&A*, 536, A89
- Hahn O., Martizzi D., Wu H.-Y., Evrard A. E., Teyssier R., Wechsler R. H., 2017, *MNRAS*, 470, 166
- Hutchings J. B., Neff S. G., 1991, *AJ*, 101, 2001
- Kale R., Parekh V., 2016, *MNRAS*, 459, 2940
- Lacy M., Rawlings S., Hill G. J., 1992, *MNRAS*, 258, 828
- Mazzotta P., Giacintucci S., 2008, *ApJ*, 675, L9
- Munari E., Biviano A., Borgani S., Murante G., Fabjan D., 2013, *MNRAS*, 430, 2638
- Parekh V., van der Heyden K., Ferrari C., Angus G., Holwerda B., 2015, *A&A*, 575, A127
- Pinkney J., Roettiger K., Burns J. O., Bird C. M., 1996, *ApJS*, 104, 1
- Pisani A., 1993, *MNRAS*, 265, 706
- Pisani A., 1996, *MNRAS*, 278, 697
- Poole G. B., Babul A., McCarthy I. G., Sanderson A. J. R., Fardal M. A., 2008, *MNRAS*, 391, 1163
- Ramella M., Boschin W., Fadda D., Nonino M., 2001, *A&A*, 368, 776
- Reynolds C. S., Lohfink A. M., Babul A., Fabian A. C., Hlavacek-Larrondo J., Russell H. R., Walker S. A., 2014, *ApJ*, 792, L41
- Roettiger K., Loken C., Burns J. O., 1997, *ApJS*, 109, 307
- Russell H. R., Fabian A. C., Sanders J. S., Johnstone R. M., Blundell K. M., Brandt W. N., Crawford C. S., 2010, *MNRAS*, 402, 1561
- Savini F. et al., 2018, *MNRAS*, 478, 2234
- Schneider D. P., Bahcall J. N., Gunn J. E., Dressler A., 1992, *AJ*, 103, 1047
- Serna A., Gerbal D., 1996, *A&A*, 309, 65
- Sommer M. W. et al., 2017, *MNRAS*, 466, 966
- Tonry J., Davis M., 1979, *ApJ*, 84, 1511
- Venturi T. et al., 2017, *A&A*, 603, A125
- Walker S. A., Fabian A. C., Russell H. R., Sanders J. S., 2014, *MNRAS*, 442, 2809
- Wold M., Lacy M., Dahle H., Lilje P. B., Ridgway S. E., 2002, *MNRAS*, 335, 1017
- ZuHone J., Markevitch M., Brunetti G., Giacintucci S., 2013, *ApJ*, 762, 78

This paper has been typeset from a  $\text{\TeX}/\text{\LaTeX}$  file prepared by the author.